nature materials

ARTICLES

https://doi.org/10.1038/s41563-022-01319-w

Check for updates

Cationic polymer-in-salt electrolytes for fast metal ion conduction and solid-state battery applications

Fangfang Chen[1,2]✉, Xiaoen Wang[1]✉, Michel Armand[3] and Maria Forsyth[1,2]✉

Polymer electrolytes provide a safe solution for future solid-state high-energy-density batteries. Materials that meet the simultaneous requirement of high ionic conductivity and high transference number remain a challenge, in particular for new battery chemistries beyond lithium such as Na, K and Mg. Herein, we demonstrate the versatility of a polymeric ionic liquid (PolyIL) as a polymer solvent to achieve this goal for both Na and K. Using molecular simulations, we predict and elucidate fast alkali metal ion transport in PolyILs through a structural diffusion mechanism in a polymer-in-salt environment, facilitating a high metal ion transference number simultaneously. Experimental validation of these computationally designed Na and K polymer electrolytes shows good ionic conductivities up to 1.0×10^{-3} S cm^{-1} at 80 °C and a Na^+ transference number of ~0.57. An electrochemical cycling test on a Na|2:1 NaFSI/PolyIL|Na symmetric cell also demonstrates an overpotential of 100 mV at a current density of 0.5 mA cm^{-2} and stable long-term Na plating/stripping performance of more than 100 hours. PolyIL-based polymer-in-salt strategies for new solid-state electrolytes thus offer an alternative route to design high-performance next-generation sustainable battery chemistries.

High-energy-density energy storage technology requires a new generation of anode materials, for example alkali metal anodes (Li, Na or K) with high theoretical capacities. Such reactive anodes necessitate the discovery of compatible electrolyte materials to support the safe and long-term cycling of the devices. Polymer electrolytes (PEs) are now accepted as an enabler of the ultimate solid-state high-performance batteries[1–4], thanks to their great advantages in suppressing both the explosion risk and uncontrollable dendrite formation, in addition to their high thermal and electrochemical stabilities and advantages in fabrication.

The earliest PEs based on polyethylene oxide (PEO) and its copolymers have been extensively studied[5–9]. The key challenges associated with those PEs are to achieve high ionic conductivity (σ) and high Li^+ transference number (t_{Li}) simultaneously, and the stable cycling of solid-state batteries[6]. Those materials normally have low conductivities or lower t_{Li} (~0.2), which are intrinsically related to their structures (for example, strong coordination of metal ions with polar groups in polymer backbones)[10–12]. A variety of polymer design strategies have been proposed to improve metal ion transport and transference number. For example, the introduction of loosely coordinating repeat units (for example, polycarbonates, polyesters or poly(tetrahydrofuran)) can enhance Li^+ or Na^+ migration, with high transference numbers (>0.5) achieved[12–16]. Designing new anion chemistries with restricted motions also can increase the Li^+ transference number[17]. Using block copolymers or crosslinking polymer chains is another way to improve ionic conductivities[18]. Aside from those methods, the search for new polymer materials with higher metal ion transference numbers and conductivities is ongoing.

One approach to maximize the metal ion transference number is to use polyanionic materials, in which anions are chemically bonded to polymer backbones, and cation (for example, Li^+) conduction dominates so that the cation transference number tends to unity[19]. This situation is highly desirable in batteries to overcome problems related to anion concentration gradients. Despite progress, such single-ion conductors still typically suffer from very low ionic conductivities that hinder their application[20].

Recently, cationic PEs named polymeric ionic liquids (PolyILs)[21], in which the monomer is a polymerizable ionic liquid cation, have emerged as potential solid-state solvents for lithium salts and shown good performance[22,23]. This material inherits both the excellent electrochemical performance of ionic liquids and the good thermal and mechanical properties of polymers[24,25]. Interestingly, due to a unique Li–anion–polycation co-coordination structure[26], the ionic conductivity of these materials increases with increasing salt concentrations[26], which is very different from conventional PEs. This positive relationship is in line with the 'polymer-in-salt' electrolytes[27–29] proposed by C. Austen Angell decades ago. In such electrolytes, once the salt is the dominant component, the ion mobility will begin to increase again while the glass transition temperature (T_g) decreases[27]. However, the PolyIL is unique in that this positive relationship is also applicable to the low salt concentration range, and high conductivities and high t_{Li} have been obtained simultaneously in PolyIL-in-salt (PolyIL-IS)[26].

Recent computational research suggested a vehicular Li^+ diffusion mechanism in PolyIL electrolytes that, however, focused on a low to medium salt concentration range (that is, Li^+/polycation unit ≤ 0.4)[30]. This mechanism is likely to be concentration dependent because the salt concentration will alter the Li^+ coordination environment and thus its transport as demonstrated in liquid electrolytes[31–37]. Given the recent promising demonstration of the PolyIL-IS system in Li metal batteries, understanding the ion transport of other, more abundant metal cations in such materials can open up the possibility for designing high-performance solid-state batteries based on the PolyIL-IS platform.

[1]Institute for Frontier Materials, Deakin University, Geelong, VIC, Australia. [2]ARC Centre of Excellence for Electromaterials Science (ACES), Deakin University, Burwood, VIC, Australia. [3]CIC EnergiGUNE, Basque Research and Technology Alliance (BRTA), Vitoria-Gasteiz, Spain. ✉e-mail: fangfang.chen@deakin.edu.au; xiaoen.wang@deakin.edu.au; maria.forsyth@deakin.edu.au

Thus, in this work, we present a computational design of PolyIL-IS electrolytes, investigating the transport of Na^+ and K^+. We discovered a rapid diffusion of alkali metal ions through a structural diffusion mechanism. Under the premise of weak interaction between metal ions and anions, the salt-concentrated environment favours fast metal ion diffusion at 80 °C. We also investigated the diffusion of the multivalent Mg^{2+} in these PolyIL-IS systems and discussed the challenges in achieving high Mg^{2+} conduction. Finally, as a proof of concept, we validated the computational findings by experimental measurement. In the preliminary test of a Na-based PolyIL-IS electrolyte (with mechanical reinforcement), we showed high ionic conductivities and excellent stable cycling behaviour in a sodium symmetric cell. Thus, this solid, solvent-free PolyIL-IS opens up an avenue for developing safer high-energy-density batteries.

Computational design of optimal PolyIL-IS systems

The PolyIL studied in this work is poly(diallyldimethylammonium) bis(fluorosulfonyl)imide (PDADMA FSI; Supplementary Fig. 1e). Our previous work has studied this polymer with the LiFSI salt[26]. Careful experimental measurements of various polycation/Li ratios from 2:1 to 1:6 have determined the ratio to achieve the optimum conductivity, which is 1:1.5. However, such an approach to electrolyte design is both time consuming and costly, and here we sought a more efficient computational approach to design the Na, K and Mg systems. Based on our earlier molecular dynamics (MD) simulations of Li systems, the optimal 1:1.5 ratio allows the most Li^+ to be homogeneously distributed around PDADMA backbones by co-coordinating with anions. At higher Li^+ ratios, molten salt-like aggregates form, which are shown in silico to enhance Li^+ diffusion. However, in experiments, these aggregates eventually transform into the less conductive crystalline phases, which are slow to form, and thus, this final stable state is far from attainable within the MD simulation timescale. Nevertheless, based on these understandings, we hypothesize here that a close-to-optimal salt concentration could at least be identified from a PolyIL-IS composition that gives the 'saturated' metal ion distribution around polymer chains. This can be determined via quantifying three anion coordination states (Fig. 1a): (1) polycation–anion coordination (P^+–A^-) as seen in neat PolyIL or with low salt concentrations; (2) metal ion–anion coordination (Me^+–A^-) as seen in the molten salt-like regime; and (3) polycation–anion–metal ion co-coordination (P^+–A^-–Me^+). The coordination of two ions is determined by measuring their distance, which should be less than the first prominent valley distance in their radial distribution function (RDF; explained in Supplementary Fig. 2, Supplementary Table 1 and Supplementary Note 1).

For the Na system, two cation ratios of 1:2 and 1:4 were first simulated at 353 K (termed Na12 and Na14). The 1:2 was chosen as it is close to the optimal ratio of the Li system and Na^+ also coordinates with a slightly higher number of FSI^- than Li^+. The higher salt ratio of 1:4 was also examined. The snapshots in Fig. 1b show the selected structures of the two equilibrated Na systems, which present the FSI^- only in P^+–FSI^- (purple) and Na^+–FSI^- (green) states. The percentage of FSI^- in both single coordination states in Na12 is very low, resulting in the highest co-coordinated FSI^- of 97%, exceeding the 92% co-coordination percentage in 1:1.5 PolyIL/LiFSI. Therefore, the 1:2 ratio could be an optimal ratio for Na salt. For the Na14 case, with the added salt doubled, the percentage of FSI^- in the Na^+–FSI^- coordination state increases markedly to 19.7%, indicating the growth of the Na^+–FSI^--rich domains, and this change is consistent with the LiFSI study[26].

The 1:2 cation ratio was then examined for both K and Mg systems. As shown in Fig. 1c and the snapshots in Supplementary Fig. 1, the percentage of FSI^- in the FSI^-–Me^+ coordination state is 8% and 23.1% for K12 and Mg12, respectively, suggesting the existence of the excessive K and Mg salts; lower salt concentrations should be examined next to increase the co-coordination state. As expected, at a 1:1 ratio, the co-coordination state in K11 and Mg11 increases from 91% and 73.9% to 94% and 85.4%, respectively.

The cation ratios to give the maximum co-coordination anion state are 1:1.5, 1:2 and 1:1 for Li^+, Na^+ and K^+, respectively. Interestingly, this order does not follow the order of the three alkali elements in the periodic table, but may be related to the different cation–anion coordination abilities. For example, when comparing the coordination numbers (CNs; Supplementary Table 1) between Na12 and K12, the CN of P^+–FSI^- is near 9 in Na12, which is greater than the 8.1 in K12. An opposite situation occurs for the CN of Me^+–FSI^-, which is greater in K12 (6.4) than in Na12 (5.6). Therefore, the co-coordinated K^+ concentration around the polycationic backbone bridged by FSI^- should be less than the Na^+ concentration. The CN also helps us to understand the extensive Mg–FSI-enriched domains in the Mg12 system, which are explained in Supplementary Note 1, with the detailed coordination analysis of the RDF results.

The impact of the chemical environment on ion diffusion

The diffusion of ions is investigated through the mean square displacement (Supplementary Fig. 3) to evaluate the ionic conductivity in sodium, potassium and magnesium electrolytes. K12, Na12 and Mg11 that have the same anion concentration are selected and compared. In general, ion diffusion in the alkali metal ion systems is one to two orders of magnitude higher than that in the magnesium system. At 353 K, the diffusion of metal ions and anions in the K12 system is faster than that in the Na12 system. Similar results were also reported in an ionic liquid electrolyte, *N*-methyl-*N*-propylpyrrolidinium bis(fluorosulfonyl)imide (C3mpyrFSI)[38,39]; when mixed with the same amount of KFSI or NaFSI salt, the ionic liquid system with the KFSI salt has higher ionic conductivity. This may be due to the lower Lewis acidity of potassium, making its interaction with anions weaker than that of sodium, which is confirmed by the density functional theory calculation of the binding energy (E_b) between metal ions and anions.

Figure 2a plots the E_b and the diffusivity (D) of the metal ions and FSI^-. The methods of calculating E_b and D are described in Supplementary Note 2. For comparison, the diffusivity of Li^+ from the previously simulated 1:1.5 LiFSI system[26] was also calculated. The diffusion of metal ions and anions follows KFSI > NaFSI > LiFSI > MgFSI, which is in contrast with the order of E_b. Interestingly, the plotted E_b versus $\log(D)$ profile of alkali metal cations at a given temperature of 353 K shows a near-linear relationship, that is $\log(D) = AE_b + B$ (A and B are constants). If we consider that diffusion processes follow an Arrhenius or Vogel–Tammann–Fulcher relationship such that the logarithm of diffusion and the activation energy E_a at a given temperature T also follow the same type of equation, this leads to the inference of a positive correlation between the binding energy of Me^+–FSI^- and the activation energy of Me^+ diffusion, at this given temperature and salt concentration.

All alkali metal ions are more diffusive than anions, which contrasts with traditional PEO-based PEs. Considering that the polycations are immobilized, higher alkali cation transference numbers can be obtained. The opposite result is observed for the Mg^{2+} system; in addition to having the lowest ion diffusivities, Mg^{2+} is also less diffusive than FSI^-.

Next, we compared ions having distinct fast and slow diffusion (defined according to their mean square displacement values in Supplementary Fig. 4) in both Na12 and Mg11 and studied how the coordination environment affects the fast ion diffusion. Figure 2c,d calculates the RDFs of fast versus fast, fast versus slow and slow versus slow FSI^- and Na^+, first considering the correlation between their diffusion. Both fast (or both slow) FSI^- and Na^+ tend to coordinate with each other, according to their more prominent RDF peaks and higher CN values, compared to those of the fast and slow coordination. This could suggest that the movement of Na^+ and FSI^- has a strong correlation. Then, Fig. 2e,f investigates the coordination

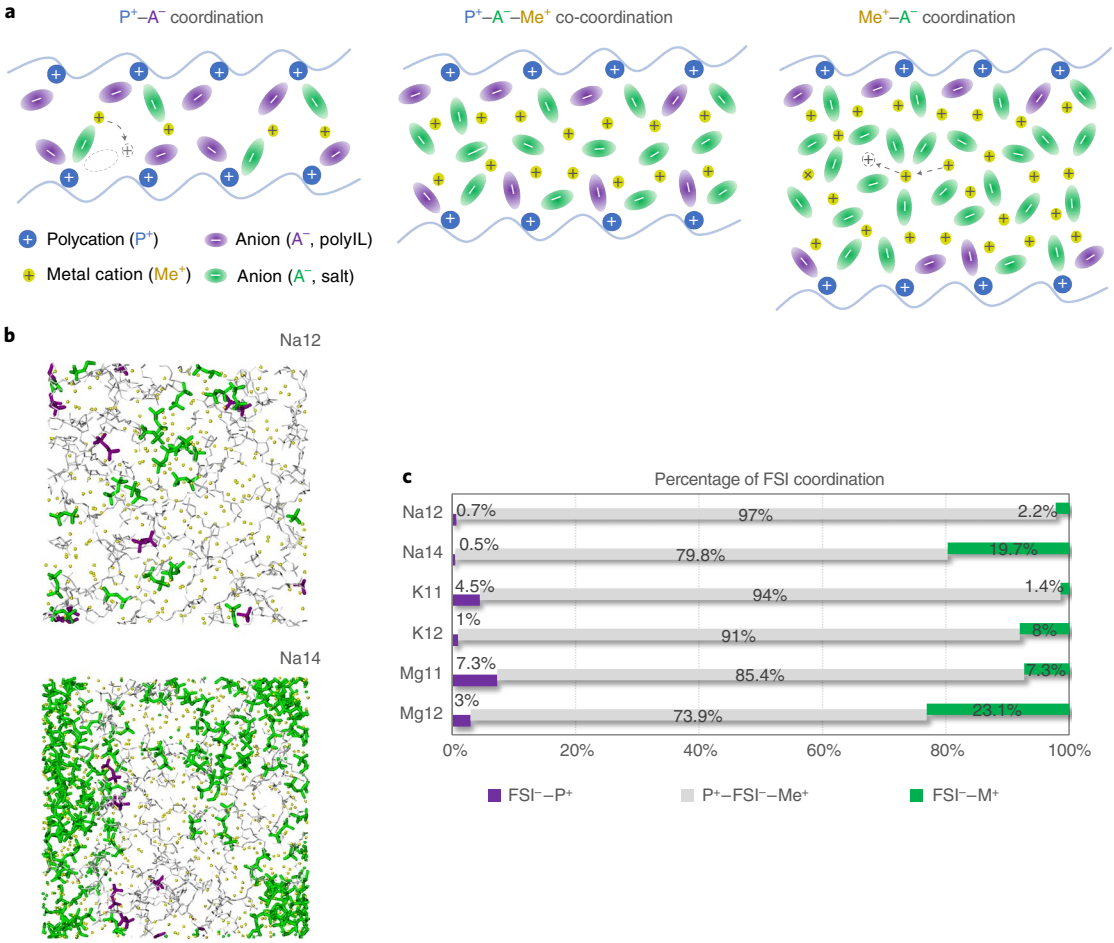

Fig. 1 | Cation–anion coordination in PolyILs. a, Schematic diagram showing the three dominant anion coordination states in PolyIL with increasing salt concentrations. The mechanism of metal ion transport at low and high salt concentrations is illustrated. Colour codes: polycation, blue; FSI^- in PolyIL, purple; FSI^- in salt, green; metal cation, yellow. **b**, Snapshots to show the equilibrium Na12 and Na14 systems. Only the FSI^- anions in the P^+–FSI^- (purple) and Na^+–FSI^- (green) states are displayed. **c**, Percentages of FSI^- in three coordination states for all investigated PolyIL systems.

of the fast or slow FSI^- and Na^+ to polycations. Both show that fast species coordinate less with polycations, while slow species tend to coordinate more with polycations. Finally, Fig. 2g,h investigates the number of Na^+ and FSI^- ions surrounding the selected fast and slow Na^+. Interestingly, there are always more Na^+ and FSI^- ions surrounding the fast Na^+; that is, the environment rich in Na^+ and FSI^- favours fast metal cation dynamics, as demonstrated by a snapshot in Fig. 2b. The fast Na^+ (red) has the molten Na–FSI salt-like chemical environment, which is commonly seen in superconcentrated ionic liquid electrolytes[31,35,40]. By contrast, the environment of the slow Na^+ (blue) contains fewer FSI^- and Na^+ within the same distance range. This suggests that the molten salt regions formed in this PolyIL can promote metal ion diffusion at 353 K, thus providing a possible theoretical guideline for future PE design, that is, by enhancing the molten salt-like domains in a PolyIL matrix. We will show some experimental evidence to validate this idea in the next section.

In the case of the Mg11 system (Supplementary Fig. 5a,b), we observe some contrasting behaviour. The fast FSI^- preferentially coordinates with the polycationic backbone. The environment of the fast Mg^{2+} is also found near the polycation rather than the domain rich in Mg^{2+} and FSI^- (Supplementary Fig 5d–f). This opposite situation can be understood by considering the binding strength between the metal ions and FSI^- (Fig. 2b). The interaction of Mg^{2+} with FSI^- is too strong to enhance the diffusion of both. Therefore, the ionic conductivity enhancement in PolyIL-IS requires the metal ion–anion interaction to be weak enough to allow fast exchange in the coordination environment, which we discuss in more detail below. For the development of PolyIL capable of conducting multivalent ions (for example, Mg^{2+}, Zn^{2+} and so on), one key is to reduce the metal ion–anion binding strength to a similar magnitude as that of the alkali metal ion–anion.

Metal ion diffusion mechanisms

In this section, we show that the alkali metal ions in the PolyIL-IS system diffuse mainly through a structural diffusion mechanism, as opposed to the vehicular diffusion mechanism suggested for the low salt concentration PolyIL[30]. Briefly speaking, 'vehicular diffusion' refers to the transport of metal ions together with their ligands, and 'hopping' refers to complete and direct ligand exchange, whereas 'structural diffusion' refers to the transport of metal ions through the partial exchange of ligands. However, the diffusion mechanism of metal ions here is also distinguished from 'the directly coupled ionic mobility' in traditional PEs, such as PEO, where the ligands (that is, polar groups in the backbone) are also partly exchanged during the metal ion diffusion process (Supplementary Fig. 6a). The metal ions in PolyIL can not coordinate directly with the cationic polymer backbones; instead, bridging coordination through anions occurs. Therefore, metal cations still diffuse through anion exchange. The impact of structure/segmental relaxation of polymer chains on metal ion dynamics is indirect and could be substantially affected

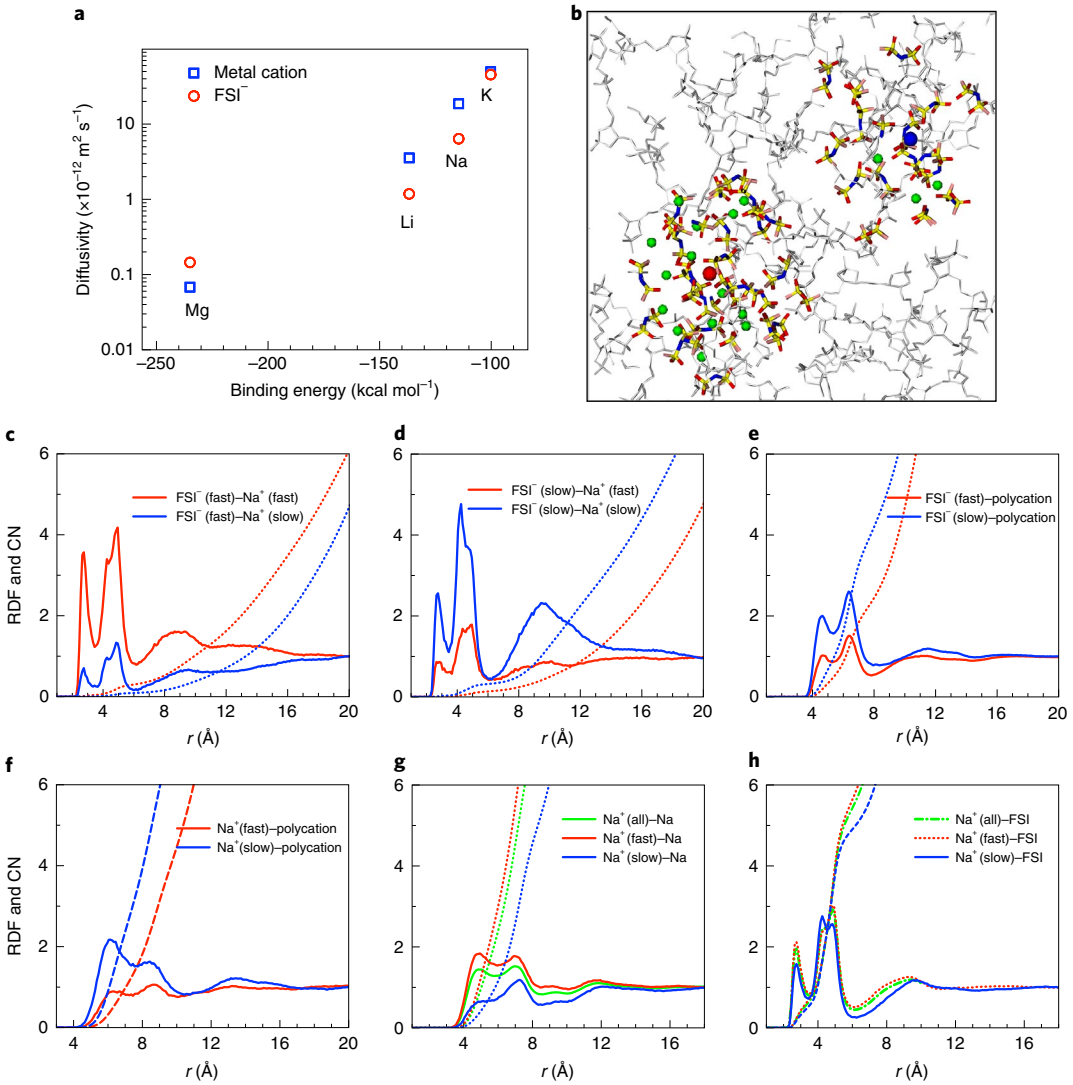

Fig. 2 | Diffusion of ions and analysis of the correlation between fast or slow ions. a, Log plot of diffusivity as a function of binding energy (E_b) of Me^+–FSI^- for the K12, Na12, Mg11 and Li (1:1.5) systems. **b**, A snapshot to show fast (red) and slow (blue) Na^+ and their respective chemical environments; the surrounding FSI^- (bold sticks) and Na^+ (green balls) are highlighted. **c**,**d**, RDF and CN of fast/slow FSI^- with fast/slow Na^+. **e**,**f**, RDF and CN of fast/slow FSI^- or Na^+ with polycations; **g**,**h**, RDF and CN calculated between fast/slow/all Na^+ with Na^+ or FSI^-. RDF and CN are plotted with solid and dotted lines, respectively, and share the same y-axis scale.

by salt concentration. At low salt concentrations, all anions coordinate with polycations and polymer segmental movement can affect anion movement and thus affects the motion of the co-coordinated metal ions (Fig. 1a)[30]. However, at high salt concentrations, such as Na14 and K12 (Fig. 1c), anions either weakly co-coordinate with polycations (binding energy calculation in Supplementary Fig. 6b) or coordinate only with metal ions in a molten salt region; the metal ion diffusion may become more decoupled from polymer segmental motion in this case. Therefore, the diffusion mechanism of metal ions in PolyIL-IS is very similar to that in the salt-concentrated ionic liquids where there are metal ion–anion aggregates, and a structural diffusion mechanism takes place.

The structural diffusion mechanism can be studied by tracing the coordinated anions (or ligands) of a given metal cation during its diffusion. If we consider a coordination shell as a 'cage', we can quantitatively determine the cage restructure and its connection to the metal ion diffusion processes. We define 'a cage-restructure period' (Fig. 3a) as the period between the formation of an initial cage A and the formation of a new cage B. In terms of 'vehicular mechanism', this period will be sufficiently long so that the metal ions mainly diffuse with the cage. By contrast, this period for a 'structural mechanism' should be much shorter, with the result that the diffusion of ions occurs through the cage restructuring. For the 'hopping mechanism', the anion exchange occurs instantaneously and causes ion migration via a hop from one cage to another.

In Fig. 3b, the metal ion cage restructuring is analysed for Na12 and K12 through a self-defined cage-restructure correlation function $C(t)$ based on a cage-state function $h(t)$ illustrated in Fig. 3a (the definition of $C(t)$ is described in Supplementary Note 2; t, time). The decay in this function reflects the restructure of the cage, that is, the original anions being partially or completely replaced. This function decays to zero when all metal ions have a new cage. $C(t)$ decays to 0.9 almost immediately for both K12 and Na12. It takes 3.5 ns to decrease to 0.01 in K12, which is much faster than in Na12, which requires the 12.7 ns.

Figure 3c,e analyses the distance the Na or K travels during a cage-restructure period. For all cage-restructure periods using the same time, their frequency of occurrence is counted, and the

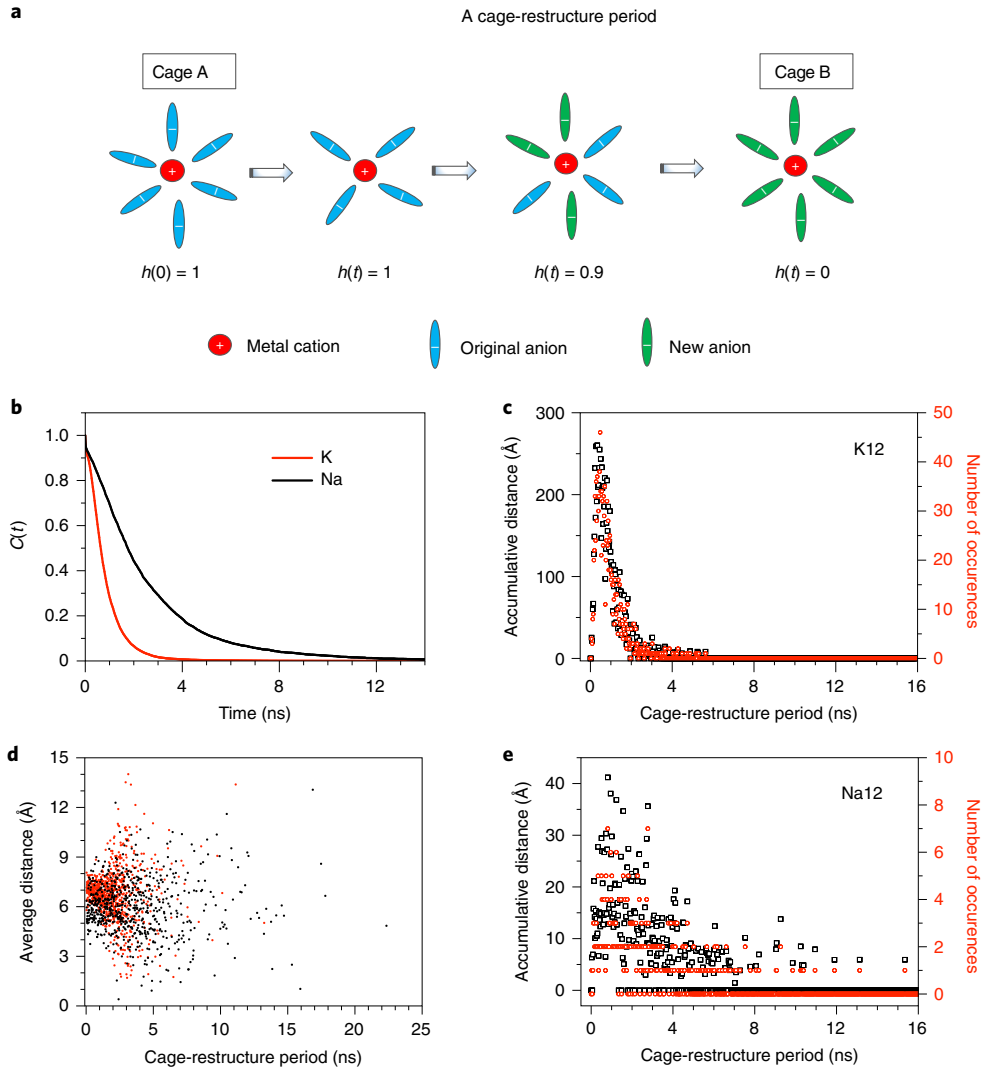

Fig. 3 | Analysis of metal ion cage restructure and ion transport for the K12 and Na12 systems. a, Illustration of a cage-restructure period and the corresponding coordination state function $h(t)$. **b**, Cage-restructure correlation functions of Na and K. **c**, The number of occurrences of cage restructure by time of restructure period, and accumulative travel distances of K^+ during all the same restructure periods. **d**, The average travel distance of Na^+ (black) and K^+ (red) in different cage-restructure periods. **e**, The number of occurrences of cage restructure by restructure period time, and accumulative travel distances of Na^+ during all the same restructure periods.

distance the metal ions move is accumulated. The distributions of accumulative distances and frequencies present similar patterns, indicating a positive correlation between the two quantities. The average distance is calculated in Fig. 3d by dividing the accumulative distance by the frequency. No linear dependence between average travel distance and cage-restructure time is seen. Therefore accelerating the frequency of the cage restructure is more important for promoting metal ion diffusion, which should be a key to achieving high conductivity through the structural diffusion mechanism.

Finally, the frequency of an instant hopping event was identified to evaluate the hopping diffusion mechanism. This is when the cage restructuring is completed between two consecutive frames in the MD trajectory. Only seven events were detected in more than two million inspections, indicating that this mechanism would only rarely contribute to diffusion, and thereby ionic conductivity, in these electrolytes.

Experimental validation of in silico predictions

Based on simulation results, we conducted experimental validations on Na11, Na12, Na13, Na14, K11 and K12 to verify the composition dependence and high ion conductivities in PolyIL-IS. The electrolytes were prepared according to Supplementary Note 3. Figure 4a compares the T_g values of the Na, K and previously investigated Li systems[26]. T_g is normally used as an indicator of ion dynamics of PEs whose ion dynamics are highly correlated with the relaxation process of the polymer backbones. For PolyIL systems, T_g decreases with increasing salt concentration; for example, Na11 > Na12 > Na14 (Fig. 4a and Supplementary Fig. 7b–d). This is due to the increase in metal ion–anion–polycation co-coordination, which reduces not only the ionic crosslinking of polymer chains but also the polycation–anion interaction (from −293.47 to −62.6 (−50.5) kJ mol^{-1} when a Na^+ (Li^+) is attached to FSI^-, according to the density functional theory binding energy calculations in Supplementary Fig 6b), thereby increasing the local dynamics that control T_g. In the case of Na, the decrease of T_g is most pronounced from Na11 to Na12, and the change is no longer obvious with the increase of salt concentration after Na12 obtains the highest anion co-coordination state. The T_g values of the lithium systems are overall the lowest, which may be due to the strong Li–anion binding energy, resulting in the weakest polycation–anion interaction. However, the highest T_g values of the

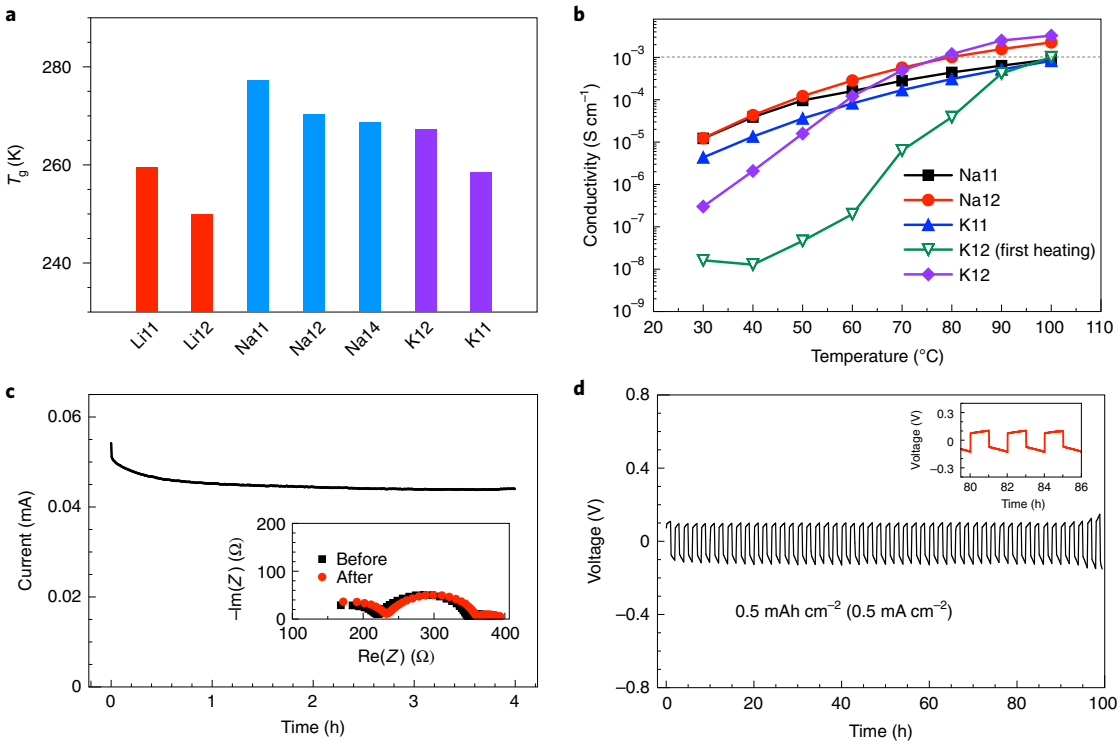

Fig. 4 | The thermal properties, ionic conductivities and electrochemical properties of PDADMA-based PEs. a, Glass transition temperatures (T_g) of PolyILs with various salts and concentrations. **b**, Ionic conductivities as a function of temperature for Na- and K-based PolyIL PEs. **c**, The chronoamperometry profile of a Na/Na12 PE/Na symmetric cell with a constant polarization voltage of 20 mV. Inset shows the Nyquist plots (the negative imaginary part versus the real part of the impedance Z) of the cell before and after polarization. **d**, Na plating/stripping for a Na/Na12 PE/Na symmetric cell with an applied current density of 0.5 mA cm^{-2} and an areal capacity of 0.5 mAh cm^{-2}. Inset shows the zoom-in picture between 79 and 86 hours. The electrochemical tests in **c** and **d** were performed at 80 °C.

Na systems suggest that the metal ion–anion binding strength is not the sole decisive factor.

The conductivity was measured for Na11, Na12, K11 and K12 in Fig. 4b. Na12 has the highest overall conductivity ranging from 10^{-5} to over 10^{-3} S cm^{-1} between 30 and 100 °C. Notably, these values are comparable to that of LiTFSI(PEO)$_{20}$ (ref. [41]) and NaTFSI(PEO)$_9$ (ref. [8]), which are between 4.5×10^{-6} and 3×10^{-4} S cm^{-1} from 20 to 70 °C. Na12 has higher conductivity than Na11, which is consistent with the MD prediction and corresponds to its lower T_g.

The conductivities of the K systems are greatly affected by the heat treatment history. They have overall lower conductivities during the first heating cycle than the Na systems. K11 also has higher conductivities than K12, which does not correspond to its lower T_g. This should be due to the presence of a second crystalline phase as indicated by differential scanning calorimetry measurements (Supplementary Fig. 7a), as we previously noted in the Li systems when the polycation/Li ratio is higher than 1:1.5 (ref. [26]). Encouragingly, the disappearance of the crystalline phase during the second heating cycle remarkably increases the conductivity of K12, which exceeds all other systems from 80 °C, and this supports the MD predictions. Note that only the amorphous phase was obtained within the MD simulation time limit, and this also suggests that maintaining a single, amorphous polymer phase is essential to ensure high ionic conductivity in these superconcentrated systems. The conductivity results at low temperatures also suggest that the ion dynamics are not conclusively predicted by the binding energy of Me$^+$–FSI. Interestingly, neither does it completely correlate with the T_g, as observed in Fig. 4a,b, where the sodium systems have the overall highest T_g and conductivities. Li12, on the other hand, has the lowest T_g and an ionic conductivity around 0.7×10^{-4} S cm^{-1} at 80 °C, which is lower than that of Na12 (1.02×10^{-3} S cm^{-1}) or K12 (1.2×10^{-3} S cm^{-1} at second heating).

The Arrhenius plots of conductivities in Supplementary Fig. 8a show positive curves, indicating that the metal ion conduction mechanism is not through hopping, as confirmed by MD analysis. The Vogel–Tammann–Fulcher plots of conductivities in Supplementary Fig. 8b (and Supplementary Table 2 with discussion) show a good linear fit for Na11 and Na12, indicating that the mobile ions are somewhat coupled with the polymer. However, we note the conductivity of Na12 measured at 0 °C, just above T_g (−2.7 °C), when polymer motion is highly restricted, is 2.27×10^{-8} S cm^{-1} (Supplementary Fig. 8c). The decoupling index (R_τ) (the ratio of the structural relaxation time to the conductivity relaxation time) can be calculated in terms of conductivity σ at T_g based on the empirical relation $\log(R_\tau)\approx14.3+\log(\sigma(T_g))$ proposed by Angell[42]. The $\log(R_\tau)$ is as high as around 6.3, suggesting a very weak coupling between the mobile ions and the polymer matrix, as this value is close to zero for a fully coupled system[43,44].

Na12 was chosen for further electrochemical characterization. The chronoamperometry profile of the Na12 symmetric cell (Fig. 4c) and the Nyquist plots before and after d.c. polarization (inset) show that the current was maintained at a high level of 0.044 mA after a fast decay from the initial 0.054 mA in the first hour, indicating a relatively high Na$^+$ current. Further analysis via the Bruce–Vincent method confirms a Na$^+$ transference number (t_{Na}) of 0.57 at 80 °C, which is much higher than the 0.16 obtained for the PEO–NaFSI system[45]. Such a high t_{Na} is supported by MD simulations, which obtain $t_{Na}\approx0.65$ at 353 K calculated from diffusivities of ions (Supplementary Table 5 and Supplementary Note 3). Figure 4d shows the Na12 plating/stripping behaviours by a symmetric Na cell

cycling test, and long-term, stable Na plating and stripping is sustained under a high current density of 0.5 mA cm^{-2}, with the areal capacity of 0.5 mAh cm^{-2}. For solvent-free PEs, the current density applied in this case is much higher than that of state-of-the-art electrolyte systems, such as the 0.1 mA cm^{-2} that is used for PEO–NaFSI (ref. [46]). More surprisingly, the polarization voltage for the Na12 electrolyte is relatively low, around 100 mV (inset in Fig. 4d), even at such a high current density. We ascribe this superior and stable plating/stripping performance to high ionic conductivity and a high Na^+ transference number of Na12. A good oxidation stability around 4.4 V was shown by linear sweep voltammetry, suggesting the possibility of Na12 to be paired with commercial cathode materials such as $NaFePO_4$ or $Na_3V_2(PO_4)_3$, which requires further experimental verification (Supplementary Fig. 9 and limitations of the method was discussed in the Electrochemical stability window (ESW) section in Supplementary Note 3). A good mechanical property was also demonstrated for the Na12 composite (Supplementary Fig. 11 and Supplementary Table 6).

The extra tests on Na14, which has more molten salt domains, also show promising results, including a higher steady-state Na^+ current at 0.064 mA (initial current, 0.084 mA); a higher Na transference number of 0.63 at 80 °C; and the potential of cycling at high current densities (Supplementary Fig. 10). However, the molten salt regime is metastable and transforms through crystallization after a few days, and thus future work will focus on stabilizing such systems. Some strategies proposed in previous studies on polymer-in-salt systems can be considered as future directions, including the use of mixed salts[47,48] or of the low-melting-temperature, weak-coordination salts[28] that we and others are currently studying.

In summary, we demonstrate that PolyIL-IS systems have the versatility for the design of solid PEs for multiple battery chemistries, including Li, Na and K, and can achieve high metal ion transport and transference number. The optimal compositions can be studied more efficiently by computationally searching for the salt concentration that can achieve the maximum anionic co-coordination state. Specifically, a structural diffusion mechanism is proposed for metal ions in the PolyIL-IS system, and rapid restructuring of the metal ion coordination cage is critical to achieving high metal ion diffusivity. The evolution of a molten salt-like region within the PolyIL facilitates rapid metal ion diffusion, provided that the binding energy of the salt is not excessive. Finally, the computational predictions are verified experimentally, and the Na12 system achieves an excellent performance, thus demonstrating the broad potential of this polymer system for the development of future all-solid-state high-energy-density batteries. This work also opens up a cost-effective computational approach to the composition design of PolyILs.

Online content

Any methods, additional references, Nature Research reporting summaries, source data, extended data, supplementary information, acknowledgements, peer review information; details of author contributions and competing interests; and statements of data and code availability are available at https://doi.org/10.1038/s41563-022-01319-w.

Received: 16 May 2021; Accepted: 20 June 2022;
Published online: 28 July 2022

References

1. Lopez, J., Mackanic, D. G., Cui, Y. & Bao, Z. Designing polymers for advanced battery chemistries. *Nat. Rev. Mater.* **4**, 312–330 (2019).
2. Zhao, Q., Stalin, S., Zhao, C.-Z. & Archer, L. A. Designing solid-state electrolytes for safe, energy-dense batteries. *Nat. Rev. Mater.* **5**, 229–252 (2020).
3. Li, J. et al. Polymers in lithium-ion and lithium metal batteries. *Adv. Energy Mater.* **11**, 2003239 (2021).
4. Mauger, A., Armand, M., Julien, C. M. & Zaghib, K. Challenges and issues facing lithium metal for solid-state rechargeable batteries. *J. Power Sources* **353**, 333–342 (2017).
5. Armand, M. The history of polymer electrolytes. *Solid State Ion.* **69**, 309–319 (1994).
6. Xue, Z., He, D. & Xie, X. Poly(ethylene oxide)-based electrolytes for lithium-ion batteries. *J. Mater. Chem. A* **3**, 19218–19253 (2015).
7. Diddens, D., Heuer, A. & Borodin, O. Understanding the lithium transport within a Rouse-based model for a PEO/LiTFSI polymer electrolyte. *Macromolecules* **43**, 2028–2036 (2010).
8. Boschin, A. & Johansson, P. Characterization of NaX (X: TFSI, FSI) – PEO based solid polymer electrolytes for sodium batteries. *Electrochim. Acta* **175**, 124–133 (2015).
9. Molinari, N., Mailoa, J. P. & Kozinsky, B. Effect of salt concentration on ion clustering and transport in polymer solid electrolytes: a molecular dynamics study of PEO–LiTFSI. *Chem. Mater.* **30**, 6298–6306 (2018).
10. Rosenwinkel, M. P. & Schönhoff, M. Lithium transference numbers in PEO/LiTFSA electrolytes determined by electrophoretic NMR. *J. Electrochem. Soc.* **166**, A1977–A1983 (2019).
11. Zhao, Y. et al. Solid polymer electrolytes with high conductivity and transference number of Li ions for Li-based rechargeable batteries. *Adv. Sci.* **8**, 2003675 (2021).
12. Zhao, Y. et al. Design strategies for polymer electrolytes with ether and carbonate groups for solid-state lithium metal batteries. *Chem. Mater.* **32**, 6811–6830 (2020).
13. Tominaga, Y. Ion-conductive polymer electrolytes based on poly(ethylene carbonate) and its derivatives. *Polym. J.* **49**, 291–299 (2017).
14. Mackanic, D. G. et al. Crosslinked poly(tetrahydrofuran) as a loosely coordinating polymer electrolyte. *Adv. Energy Mater.* **8**, 1800703 (2018).
15. Sångeland, C., Younesi, R., Mindemark, J. & Brandell, D. Towards room temperature operation of all-solid-state Na-ion batteries through polyester–polycarbonate-based polymer electrolytes. *Energy Storage Mater.* **19**, 31–38 (2019).
16. Webb, M. A. et al. Systematic computational and experimental investigation of lithium-ion transport mechanisms in polyester-based polymer electrolytes. *ACS Cent. Sci.* **1**, 198–205 (2015).
17. Zhang, H. et al. Suppressed mobility of negative charges in polymer electrolytes with an ether-functionalized anion. *Angew. Chem. Int. Ed.* **58**, 12070–12075 (2019).
18. Ben youcef, H., Garcia-Calvo, O., Lago, N., Devaraj, S. & Armand, M. Cross-linked solid polymer electrolyte for all-solid-state rechargeable lithium batteries. *Electrochim. Acta* **220**, 587–594 (2016).
19. Bouchet, R. et al. Single-ion BAB triblock copolymers as highly efficient electrolytes for lithium-metal batteries. *Nat. Mater.* **12**, 452–457 (2013).
20. Zhang, H. et al. Single lithium-ion conducting solid polymer electrolytes: advances and perspectives. *Chem. Soc. Rev.* **46**, 797–815 (2017).
21. Ohno, H., Yoshizawa, M. & Ogihara, W. Development of new class of ion conductive polymers based on ionic liquids. *Electrochim. Acta* **50**, 255–261 (2004).
22. Girard, G. M. A. et al. Sustainable, dendrite free lithium-metal electrode cycling achieved with polymer composite electrolytes based on a poly(ionic liquid) host. *Batter. Supercaps* **2**, 229–239 (2019).
23. Wang, X. et al. Poly(ionic liquid)s/electrospun nanofiber composite polymer electrolytes for high energy density and safe Li metal batteries. *ACS Appl. Energy Mater.* **2**, 6237–6245 (2019).
24. Zhang, S.-Y. et al. Poly(ionic liquid) composites. *Chem. Soc. Rev.* **49**, 1726–1755 (2020).
25. Mecerreyes, D. Polymeric ionic liquids: broadening the properties and applications of polyelectrolytes. *Prog. Polym. Sci.* **36**, 1629–1648 (2011).
26. Wang, X. et al. Poly(ionic liquid)s-in-salt electrolytes with co-coordination-assisted lithium-ion transport for safe batteries. *Joule* **3**, 2687–2702 (2019).
27. Angell, C. A., Liu, C. & Sanchez, E. Rubbery solid electrolytes with dominant cationic transport and high ambient conductivity. *Nature* **362**, 137–139 (1993).
28. Xu, W., Wang, L.-M. & Angell, C. A. "PolyMOB"–lithium salt complexes: from salt-in-polymer to polymer-in-salt electrolytes. *Electrochim. Acta* **48**, 2037–2045 (2003).
29. Forsyth, M., Sun, J., Macfarlane, D. R. & Hill, A. J. Compositional dependence of free volume in PAN/$LiCF_3SO_3$ polymer-in-salt electrolytes and the effect on ionic conductivity. *J. Polym. Sci. B Polym. Phys.* **38**, 341–350 (2000).
30. Zhang, Z., Nasrabadi, A. T., Aryal, D. & Ganesan, V. Mechanisms of ion transport in lithium salt-doped polymeric ionic liquid electrolytes. *Macromolecules* **53**, 6995–7008 (2020).
31. Giffin, G. A. et al. Connection between lithium coordination and lithium diffusion in [Pyr_{12O1}][FTFSI] ionic liquid electrolytes. *ChemSusChem* **11**, 1981–1989 (2018).

32. Kondou, S. et al. Ionic transport in highly concentrated lithium bis(fluorosulfonyl)amide electrolytes with keto ester solvents: structural implications for ion hopping conduction in liquid electrolytes. *Phys. Chem. Chem. Phys.* **21**, 5097–5105 (2019).
33. Suo, L. et al. "Water-in-salt" electrolyte enables high-voltage aqueous lithium-ion chemistries. *Science* **350**, 938–943 (2015).
34. Yamada, Y. & Yamada, A. Review—superconcentrated electrolytes for lithium batteries. *J. Electrochem. Soc.* **162**, A2406–A2423 (2015).
35. Chen, F., Howlett, P. & Forsyth, M. Na-ion solvation and high transference number in superconcentrated ionic liquid electrolytes: a theoretical approach. *J. Phys. Chem. C* **11**, 105–114 (2018).
36. Molinari, N., Mailoa, J. P. & Kozinsky, B. General trend of a negative Li effective charge in ionic liquid electrolytes. *J. Phys. Chem. Lett.* **10**, 2313–2319 (2019).
37. Gouverneur, M., Schmidt, F. & Schönhoff, M. Negative effective Li transference numbers in Li salt/ionic liquid mixtures: does Li drift in the "Wrong" direction? *Phys. Chem. Chem. Phys.* **20**, 7470–7478 (2018).
38. Matsumoto, K., Okamoto, Y., Nohira, T. & Hagiwara, R. Thermal and transport properties of Na[$N(SO_2F)_2$]–[*N*-methyl-*N*-propylpyrrolidinium] [$N(SO_2F)_2$] ionic liquids for Na secondary batteries *J. Phys. Chem. C* **119**, 7648–7655 (2015).
39. Yamamoto, T., Matsumoto, K., Hagiwara, R. & Nohira, T. Physicochemical and electrochemical properties of K[$N(SO_2F)_2$]–[*N*-methyl-*N*-propylpyrrolidinium][$N(SO_2F)_2$] ionic liquids for potassium-ion batteries. *J. Phys. Chem. C* **121**, 18450–18458 (2017).
40. Gao, X., Wu, F., Mariani, A. & Passerini, S. Concentrated ionic-liquid-based electrolytes for high-voltage lithium batteries with improved performance at room temperature. *ChemSusChem* **12**, 4185–4193 (2019).
41. Zhang, H. et al. Lithium bis(fluorosulfonyl)imide/poly(ethylene oxide) polymer electrolyte. *Electrochim. Acta* **133**, 529–538 (2014).
42. Angell, C. A. Mobile ions in amorphous solids. *Annu. Rev. Phys. Chem.* **43**, 693–717 (1992).
43. Viciosa, M. T., Diogo, H. P. & Ramos, J. J. M. The ionic liquid BmimBr: a dielectric and thermal characterization. *RSC Adv.* **3**, 5663–5672 (2013).
44. Seki, S. et al. Distinct difference in ionic transport behavior in polymer electrolytes depending on the matrix polymers and incorporated salts. *J. Phys. Chem. B* **109**, 3886–3892 (2005).
45. Ma, Q. et al. A new Na[(FSO_2)(*n*-$C_4F_9SO_2$)N]-based polymer electrolyte for solid-state sodium batteries. *J. Mater. Chem.* **5**, 7738–7743 (2017).
46. Liu, L. et al. In situ formation of a stable interface in solid-state batteries. *ACS Energy Lett.* **4**, 1650–1657 (2019).
47. Fan, J. & Angell, C. A. The preparation, conductivity, viscosity and mechanical properties of polymer electrolytes and new hybrid ionic rubber electrolytes. *Electrochim. Acta* **40**, 2397–2400 (1995).
48. Łasińska, A. K. et al. Study of ageing effects in polymer-in-salt electrolytes based on poly(acrylonitrile-co-butyl acrylate) and lithium salts. *Electrochim. Acta* **169**, 61–72 (2015).

Methods

Molecular simulations. The classic MD simulations were conducted using DL_Poly Classic software[49]. The PDADMA FSI consists of 12 PDADMA chains with each having 12 repeat cationic units and 144 FSI anions. The amount of the salt (NaFSI, KFSI or $(MgFSI)_2$) is decided according to different polycation/metal ion ratios of 1:1, 1:2 or 1:4 (given in Supplementary Table 3). All polymers and ions are randomly placed in a cubic box using Packmol[50]. The initial structures are equilibrated at 600 K and then cooled to 393 K and then 353 K. At each temperature, the system is equilibrated for 2 ns in an isothermal-isobaric *NPT* ensemble using a Berendsen thermostat and barostat with a relaxation constant of 1.0 ps each. The system is equilibrated again for 1 ns at 353 K using a Nóse–Hoover thermostat and a Hoover barostat with relaxation constants of 0.5 and 5.0 ps, respectively, and another 1 ns production run follows, for structure analysis. The velocity Verlet algorithm is adopted for integration. The time step is 1 fs and the pressure is 1 atm. The cut-offs for van der Waals force and the real space of Ewald are 12 Å. The Ewald summation method with a precision of 1×10^{-6} is used to treat the Coulomb interaction in a periodic system. All C–H bonds are constrained. A subsequent production run for dynamics analysis is conducted in a microcanonical *NVE* ensemble for 30 ns using a time step of 2.0 fs at 353 K. The equilibrium state is checked through either total energy and volume for *NPT* calculation or total temperature and pressure for *NVE* calculation, which should not increase or decrease throughout the production run. The OPLS_AA force field is used for MD simulation. The force field parameters of the FSI^- and sodium ion are taken from the CL&P force field (2018 version)[51]. Those for the PDADMA are generated using the online OPLS_AA force field generator[52] and validated in our previous work[26]. The Lennard-Jones parameters for potassium and magnesium ions are also taken from the OPLS_AA force field. A uniform scale factor of 0.7 is adopted to scale down the atomic charge in a non-polarizable force field during the MD simulation. The force field parameters, the other MD trajectory analyses and the binding energy calculation are described in Supplementary Note 2 (computational methods) and Supplementary Table 4. The limitations of classic MD simulations in materials design have been mentioned in the main text, such as being unable to simulate the new crystalline phase formation and providing only qualitative accuracy in performance predictions. Regardless, our work demonstrates that traditional MD simulations are still an important tool for materials design, providing in-depth fundamental understanding and insight into material structure and mechanisms.

Experiments. The materials and electrolyte preparation are described in Supplementary Note 3 (materials preparation and characterisations). The characterization methods of differential scanning calorimetry, ionic conductivity, dynamic mechanical analysis, transference number, electrochemical stability window and plating/stripping measurements are all given in the same section in the Supplementary Information.

Data availability

The data that support the findings of this study are available from the corresponding authors upon reasonable request. Source data are provided with this paper.

References

49. Smith, W. & Forester, T. R. DL_POLY_2.0: a general-purpose parallel molecular dynamics simulation package. *J. Mol. Graph.* **14**, 136–141 (1996).
50. Martínez, L., Andrade, R., Birgin, E. G. & Martínez, J. M. PACKMOL: a package for building initial configurations for molecular dynamics simulations. *J. Comput. Chem.* **30**, 2157–2164 (2009).
51. Lopes, J. N. C. & Padua, A. A. H. CL&P: a generic and systematic force field for ionic liquids. *Theor. Chem. Acc.* **131**, 1129 (2012).
52. Dodda, L. S., Cabeza de Vaca, I., Tirado-Rives, J. & Jorgensen, W. L. LigParGen web server: an automatic OPLS-AA parameter generator for organic ligands. *Nucleic Acids Res.* **45**, W331–W336 (2017).

Acknowledgements

F.C. and M.F. acknowledge the Australian Research Council (ARC) for funding via the ARC Centre of Excellence for Electromaterials Science, grant CE140100012. The simulation work was supported by computational resources provided by the Australian Government through the National Computational Infrastructure national facility systems under the National Computational Merit Allocation Scheme. X.W. acknowledges the financial support of the Australia-India Strategic Research Fund (AISRF 48515).

Author contributions

F.C., X.W. and M.F. conceived the idea. F.C. directed the project and conducted the computational work. X.W. conducted the experiments. The results were discussed with M.F and M.A. All authors participated in manuscript preparation.

Competing interests

The authors declare no competing interests.

Additional information

Supplementary information The online version contains supplementary material available at https://doi.org/10.1038/s41563-022-01319-w.

Correspondence and requests for materials should be addressed to Fangfang Chen, Xiaoen Wang or Maria Forsyth.

Peer review information *Nature Materials* thanks Renaud Bouchet and the other, anonymous, reviewer(s) for their contribution to the peer review of this work.

Reprints and permissions information is available at www.nature.com/reprints.